A New Variant Selection Criterion for Twin Variants in Titanium alloys (Part 1)**.

By Christophe Schuman*, Lei Bao, Jean Sébastien Lecomte, Yudong Zhang, Jean Marc Raulot, Marie Jeanne Philippe, Claude Esling

* Dr. C. Schuman
Laboratoire d'Étude des Microstructures et de Mécanique des Matériaux, LEM3, CNRS 7239, Université Paul Verlaine – Metz, Ile du Saulcy, 57045 Metz, France
E-mail : christophe.schuman@univ-metz.fr

Dr. L. Bao, J.S. Lecomte, Y. Zhang, J.M. Raulot, Prof. M.J. Philippe, C. Esling
LEM3, CNRS 7239, Université Paul Verlaine – Metz, Ile du Saulcy, 57045 Metz, France

A new selection criterion to explain the activation of the twinning variant is proposed based on the calculation of the deformation energy to create a primary twin. The calculation takes into account the effect of the grain size using a Hall-Petch type relation. This criterion allows to obtain a very good prediction for the variant selection. The calculations are compared with the experimental results obtained on T40 deformed by Channel Die compression.

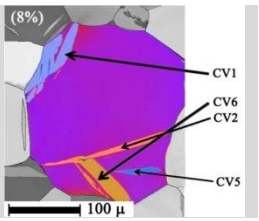

Introduction

Deformation twinning is one of the main deformation modes in crystalline solids particularly in low symmetry or multiple lattice structures [1-8]. Though extensive studies have addressed on the crystallography [9-11], morphology [12] and mechanical behavior [2, 13] of deformation twins, and numerous models for twinning have been suggested over the last few decades [14, 15], some fundamental issues remain unclear. The nucleation and growth mechanism of twin lamellae, the interaction of twinning with crystal defects, and the interfacial accommodation between the matrix and twins [16, 17] are still poorly understood.

In the case of titanium alloys, many authors have attempted to determine the presence of the different types of twins as a function of the deformation temperature or grain size [18, 19, 24] as well as to extract useful information for modeling [1, 20].

Although the twin type and the twin volume fraction can be easily determined [21], the type of variants present as well as the sequence in which they appear in one grain are not well revealed.

Recently, we have developed the "interrupted in situ SEM/EBSD orientation examination method" to follow the microstructure and crystallographic orientation evolution during the mechanical deformation process. This method allows us to obtain the time resolved information of the appearance of the twin variants, their growth, the interaction between them and the interaction with the initial grain boundaries [22]. However, the variant selection rules and the physical mechanisms behind still remain uncovered.

For magnesium and magnesium alloys that are also hexagonal materials but with different c/a ratio from that of titanium [17], Martin [26], Jonas [27] have proposed variant selection rules (Schmid Factor (SF), common volume) for the secondary twinning during deformation. Their criteria worked well for the deformed magnesium where the twins are thin. However, for titanium, it seems that the selection of the variants follows a different rule and should be clarified.

In the present work, we experimentally investigated the deformation process of commercially pure titanium with interrupted in situ SEM/EBSD orientation measurements. Based on the experimental examination, we tried to work out the twin variant selection rule. This rule is not established by a mere statistical examination to have statistical representation but to reveal the physical and mechanical criteria (energy) of variant selection that would useful for the modeling of the mechanical behavior of the alloys.

Material and Sample preparation

The material was hot-rolled and then annealed commercial pure titanium sheet of 1.5 mm thickness with the composition given in table 1.

Table 1 Chemical composition of commercially pure titanium T40

Element	H	C	N	O	Fe	Ti
Composition (ppm(wt.))	3	52	41	1062	237	Balance

A grain growth annealing was performed at 750°C for 2 hours to produce a fully recrystallized microstructure. After annealing, the samples were mechanically ground up to 4000 #-grit SiC paper and then electrolytically polished at 5°C and 17V for 30 seconds in a solution of 10 ml perchloric acid in 90 ml methanol.

The samples were channel die compressed in two passes, first with 8 % and then 16% reduction. To follow the rotation of the individual grains during the deformation, a 500×300 μm^2 area was carefully polished and marked out with four micro-indentations. The orientation of all the grains in this polished area (about 800 grains) was measured by SEM/EBSD before and after each deformation step. Fig. 1 is the sketch of the channel die compression. Before each compression, the two sample plates as shown in Fig. 1 were firmly stuck together to avoid sliding during the compression in order to maintain a good surface quality [22].

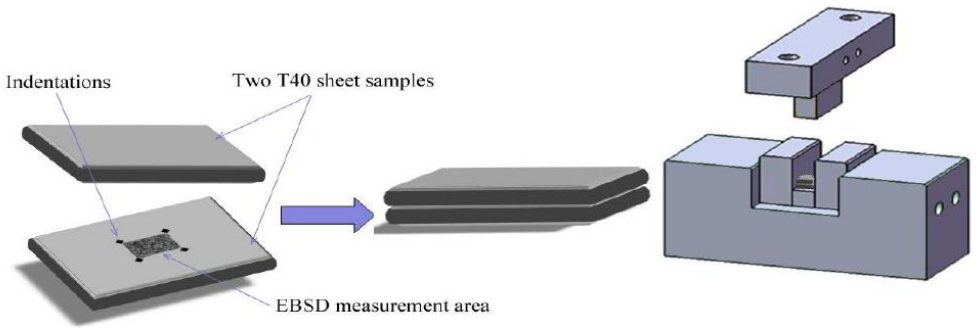

Figure 1: Schematic description of the channel-die set-up used.

Crystallography and identification

The grain size of the sample ranges from 150 to 250µm. It is well known that such large grains favour the formation of twins during deformation. We have examined more than 80 grains in this individual follow-up and identified all the twin types, their variants and their order of appearance. We found only compressive twin ($(11\bar{2}2)$ or C Type) and tension twin ($(10\bar{1}2)$ or T1 type) (see table 2), and we did not find T2 or $(11\bar{2}1)$ tension twin. The activation of these twins depends only on the initial orientation of the grain and the local stress tensor which is a function on the applied forces. Furthermore with the increase of the deformation, secondary twins appear inside primary twins: T1 tension twins inside C compression twins or C compression twins inside T1 tension twins. Generally these second generation of twins are called secondary or double twin.

Table 2: list of slip and twin systems in Titanium

Slip/Twin	$\vec{b}$	Slip system	Notation
Basal	<a>	$\{0002\}[11\bar{2}0]$	B<a>
Prismatic	<a>	$\{1\bar{1}00\}[11\bar{2}0]$	P<a>
Pyramidal π_1	<a>	$\{1\bar{1}01\}[11\bar{2}0]$	π_1<a>
Pyramidal π_1	<c+a>	$\{1\bar{1}01\}[11\bar{2}\bar{3}]$	π_1<c+a>
Pyramidal π_2	<c+a>	$\{1\bar{1}22\}[11\bar{2}\bar{3}]$	π_2<c+a>
Tension Twin	--	$\{10\bar{1}2\}[\bar{1}011]$	T1
Tension Twin	--	$\{11\bar{2}1\}[\bar{1}\,\bar{1}26]$	T2
Compression Twin	--	$\{11\bar{2}2\}[\bar{1}\,\bar{1}23]$	C

To identify the type of twin system and the active variants (Table 3) that accommodate the plastic deformation, trace analysis is used (Fig 2).

Table 3: list of variant for compression and tension twin

	Compression C									Tension T1							
	h	**k**	**i**	**l**	**u**	**v**	**t**	**w**		**h**	**k**	**i**	**l**	**u**	**v**	**t**	**w**
CV1	*1*	*1*	*-2*	*2*	*1*	*1*	*-2*	*-3*	**T1V1**	*1*	*0*	*-1*	*2*	*-1*	*0*	*1*	*1*
CV2	*-2*	*1*	*1*	*2*	*-2*	*1*	*1*	*-3*	**T1V2**	*-1*	*1*	*0*	*2*	*1*	*-1*	*0*	*1*
CV3	*-1*	*-1*	*2*	*2*	*-1*	*-1*	*2*	*-3*	**T1V3**	*-1*	*0*	*1*	*2*	*1*	*0*	*-1*	*1*
CV4	*1*	*-2*	*1*	*2*	*1*	*-2*	*1*	*-3*	**T1V4**	*0*	*-1*	*1*	*2*	*0*	*1*	*-1*	*1*
CV5	*2*	*-1*	*-1*	*2*	*2*	*-1*	*-1*	*-3*	**T1V5**	*1*	*-1*	*0*	*2*	*-1*	*1*	*0*	*1*
CV6	*-1*	*2*	*-1*	*2*	*-1*	*2*	*-1*	*-3*	**T1V6**	*0*	*1*	*-1*	*2*	*0*	*-1*	*1*	*1*

Twinning is treated as a slip system to calculate the Schmid Factor (SF). Also the trace angles of all possible twin planes on the grain surface are calculated with respect to the sample coordinate system. Then the trace angles of the observed twin planes are measured in the same coordinate system and compared with the calculated ones to identify the corresponding active twin system and twin variant. The schematic of the position of a slip line (or twin line) on the sample surface is shown in Fig 2.

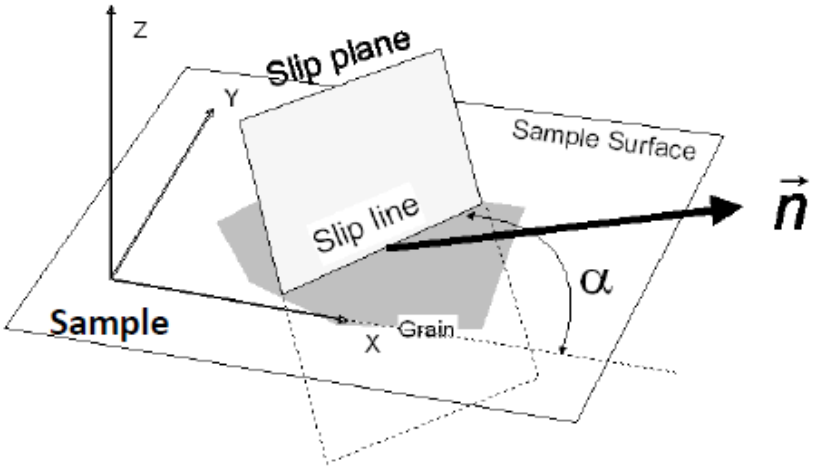

Figure 2 : Slip (twin) line trace on the sample surface.

The figure 3 follows step by step the onset of primary and secondary twin. The results show that the twin variants that appear in the grain to accommodate the deformation are seldom

those with the highest SF. In fact, only less than 50% of the variants with the highest SF are selected. Often in the equiaxed grains, several twin variants can appear, as shown in Fig. 3; whereas in those with elongated shape, only one variant appears, but it appears repeatedly, as shown in Fig. 4 b. This indicates that the shape of the initial grain also influences the selection of the variants.

We therefore decided to measure the length of each twin variant that appears (Fig. 5) and also calculate the maximum (and minimum) length of all variants that may occur to analyze the selection of the variant in terms of absorbed energy, as explained in the following.

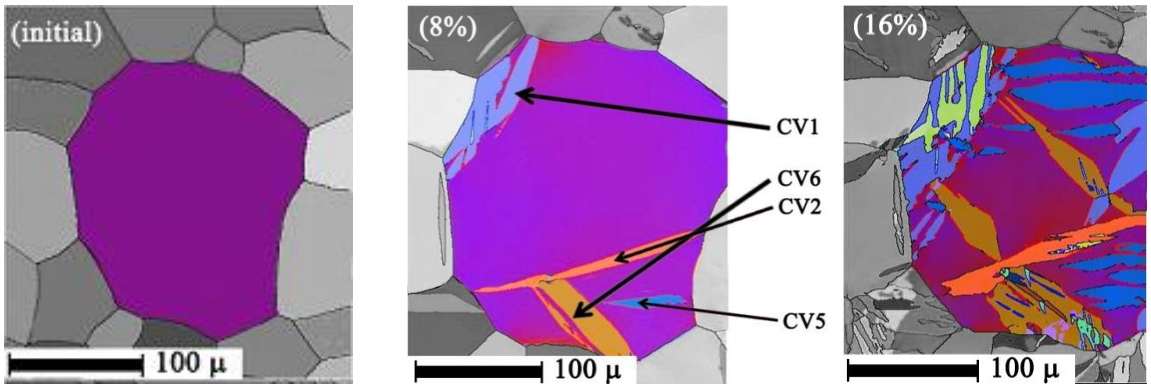

a) Orientation of the matrix :(80.0, 9.7, 39.8)

b) Several Variants appear in the grain. They appear one after another.

c) Tension Twin: T1V4. Orientation of the matrix:(69.9, 74.6, 54.9)

Figure 3: Micrographies of the same equiaxed grain at different stages of deformation.

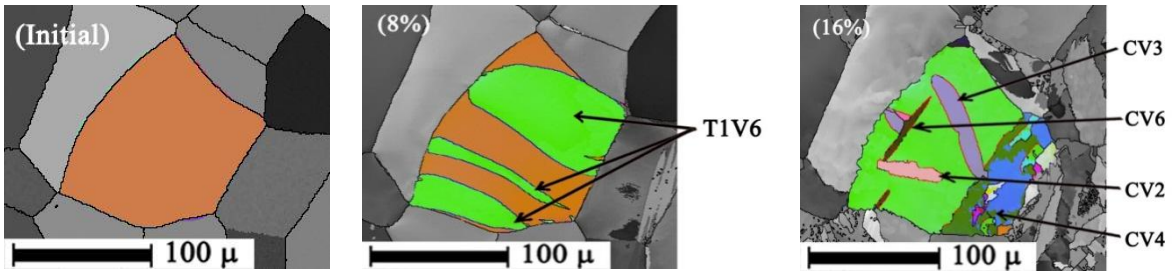

a) Orientation of the matrix :(143.4, 85.5, 11.1)

b) Tension twin : T1V6

c) Compression twin: CV4, CV2 ; CV3 ; CV6
Orientation of the matrix :(56.3, 162.5, 3.7)

Figure 4: a) initial grain; b) with one variant after 8 % deformation ; c) same grain after 16% deformation, with multiple variants

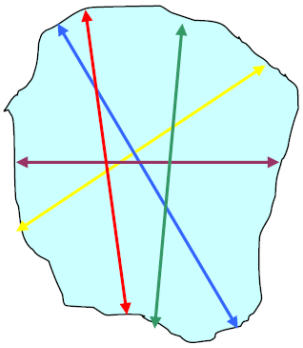

Figure 5: Sketch of a grain with orientation (x,y,z) and maximal length of the different variant.

Deformation Energy

A variant will be activated if the energy of deformation which is used to create the twin was sufficient and the internal energy of the material decreases with this operation.

We have considered here that the material is an ideal (i.e., no strain hardening) rigid- plastic body to calculate the energy of deformation. Because the elastic energy is restored when the twin is created, we restrict to the plastic energy of deformation which is calculated by the equation:

$$W_{Twin} = \sigma'_{ij}\varepsilon_{ij} \qquad (1)$$

Where σ'_{ij} is the critical resolved shear stress required (=shear stress τ in twin frame expressed in sample frame) to activate the twinning system and ε_{ij} is the corresponding twinning deformation. In the case of channel die compression, the deformation is equivalent to in-plane compression and the compressive force is applied in the sample normal direction (the third axis). In a grain, the stress applied to a twinning system is composed of the macroscopic applied stress and an additional local stress resulting from the interaction of the

considered grain with the neighboring grains. Since we restrict to relatively small deformation degrees, we neglect the local stress resulting from the interaction with the neighboring grains. The stress applied to a twinning system is thus restricted to the macroscopic compressive stress $\sigma_{33,}$ which corresponds to the Sachs (or static model) hypothesis. The twinning system will be active when the resolved shear stress reaches the corresponding critical value σ'_{33}. When the twinning system is active, the corresponding deformation energy expressed in the macroscopic coordinate system is given by the above Eq. (1).

We introduce the grain size effect by expressing the critical resolved shear stress according to a Hall Petch (HP) type equation:

$$\sigma = \sigma_0 + \frac{k}{\sqrt{L}} \qquad (2)$$

with σ_0 and k constants, σ_0 representing the stress when the length of the grain is infinite. L is the free path of the twin before encountering an obstacle (grain boundary, precipitate or other twins). Then the deformation energy can be expressed as:

$$\begin{aligned} W &= (\sigma_0 + \frac{k}{\sqrt{L}})\varepsilon_{33} \\ &= \sigma_0\varepsilon_{33} + \frac{k}{\sqrt{L}}\varepsilon_{33} \end{aligned} \qquad (3)$$

In Eq. (3), σ_0 and k are unknowns. Taking into account that twinning is activated when the size of a grain exceeds a certain value below which only crystal glide can be activated, we can deduce that the second term of the equation is dominant. Rearranging Eq. (3) we obtain:

$$\frac{W - \sigma_0\varepsilon_{33}}{k} = \frac{\varepsilon_{33}}{\sqrt{L}} \quad (4)$$

In the right hand term of Eq. (4), ε_{33} and L, are accessible to the experiment. In the following we will mainly focus on this term, $\frac{\varepsilon_{33}}{\sqrt{L}}$. Clearly, the length (L) of the free path of a twin lamella in a grain can be visualized with its boundary traces on the sample observation plane. The maximum longitudinal length of the twin lamella appearing on the sample observation plane is determined as L for each twin variant, as illustrated in Fig. 5. In the present work, the $\frac{\varepsilon_{33}}{\sqrt{L}}$ term is calculated in the sample coordinate system. For simplicity, the displacement gradient tensor

$$e_{ij} = \begin{pmatrix} \frac{\partial u}{\partial x} & \frac{\partial u}{\partial y} & \frac{\partial u}{\partial z} \\ \frac{\partial v}{\partial x} & \frac{\partial v}{\partial y} & \frac{\partial v}{\partial z} \\ \frac{\partial w}{\partial x} & \frac{\partial w}{\partial y} & \frac{\partial w}{\partial z} \end{pmatrix} \quad (5)$$

where u, v and w are the displacement components and x, y, and z are the coordinates in the sample system, was first expressed in an orthonormal reference frame defined by the related twinning elements. The unit vector normal to the twinning plane, the unit vector normal to the shear plane and the unit vector in the twinning direction define this reference frame. In this frame the displacement gradient tensor has a particularly simple form:

$$e_{ij} = \begin{pmatrix} 0 & 0 & s \\ 0 & 0 & 0 \\ 0 & 0 & 0 \end{pmatrix} \quad (6)$$

With $s = \frac{|\gamma^2-3|}{\gamma\sqrt{3}}$ for the (10-12) twin and $s = \frac{2(\gamma^2-2)}{3\gamma}$ for the (11-22) twin where $\gamma = {}^{c}/_{a}$ ratio of titanium [9], the displacement gradient tensor for the two types of twins can be obtained as:

Compression (11-22) Tension (10-12)

$$\begin{pmatrix} 0 & 0 & 0.218 \\ 0 & 0 & 0 \\ 0 & 0 & 0 \end{pmatrix} \qquad \begin{pmatrix} 0 & 0 & 0.175 \\ 0 & 0 & 0 \\ 0 & 0 & 0 \end{pmatrix} \quad (7)$$

Through coordinate transformation, this displacement gradient tensor can be expressed in the crystal coordinate system (here we choose the orthonormal reference system set to the hexagonal crystal basis and the setting follows the Channel 5 convention, i.e. $e_2//a_2$ and $e_3//c$). With the Euler angles measured by SEM/EBSD that represent a set of rotations from the sample coordinate system to the orthonormal crystal basis, this tensor can be further transformed into the macroscopic sample coordinate system. If G is the coordinate transformation matrix from the macroscopic sample coordinate system to the orthonormal twin reference system, the displacement gradient tensor with respect to the sample coordinate system can be expressed as:

$$(e_{ij}^{sample\ frame}) = G \quad (e_{ij}^{crystal\ frame})G^{-1} \quad (8)$$

Thus the deformation tensor in the macroscopic sample coordinate system can be obtained as the symmetrized displacement gradient:

$$\varepsilon_{ij} = \frac{1}{2}\left(e_{ij} + e_{ji}\right) \quad (9)$$

With Eq. (9), the energy term $\frac{\varepsilon_{33}}{\sqrt{L}}$ in Eq. (4) can thus be calculated.

Results

The energy term $\frac{\varepsilon_{33}}{\sqrt{L}}$ in Eq. (4) has been calculated for all the examined grains. We detail two cases of primary twinning, one with tension twin (T1) and the other with compression twin (C), and shown in Table 5. The examples for secondary twinning are shown in Table 6.

It should be noted that in a primary tension twin, only secondary compression twin can form and vice versa. In the table, the orientation of the grain is given by the Euler angles (φ_1, ϕ, φ_2) with respect to the macroscopic sample coordinate system are measured by EBSD/SEM. With the experimental orientation, the SF, the ε_{33} and the $\frac{\varepsilon_{33}}{\sqrt{L}}$ are calculated for all the twin variants (either tension or compression type). The $\frac{\varepsilon_{33}}{\sqrt{L}}$ is calculated using the corresponding measured grain diameter of the experimentally observed active variant is highlighted in yellow in all the tables . The maximum SF of the variants is in red. It is seen that the activated variants are not those with the highest SF but the ones with highest absolute value of $\frac{\varepsilon_{33}}{\sqrt{L}}$. The variant which has the highest local stress will consume the most energy to be activated. These results indicate that the SF as the variant selection criterion gives 45% to 50% correct prediction, whereas taking account of the mean free path gives 85%. When the initial grain is equiaxed, the free path of each variant can vary to a large extent, as shown in Fig. 3. In such a case, the activated variant is the one that has the lowest $\frac{\varepsilon_{33}}{\sqrt{L}}$ (in fact, the highest absolute ratio).

Table5: Results for primary twin

C twin	Orientation of grain:{111.5, 20.5, 34.9}				Orientation of grain:{92.4, 23.5, 35.4}			
	SF	ε_{33}	Length(μm)	$\varepsilon_{33}/\sqrt{L}$	SF	ε_{33}	Length(μm)	$\varepsilon_{33}/\sqrt{L}$
CV1	-0.479	-0.104	85	-11.3	-0.465	-0.101	115	-9.5
CV2	-0.383	-0.084	70	-10.0	-0.305	-0.067	81	-7.4
CV3	-0.222	-0.048	95	-5.0	-0.152	-0.033	120	-3.0
CV4	-0.242	-0.053	90	-5.6	-0.260	-0.057	105	-5.5
CV5	-0.407	-0.089	70	-10.6	-0.431	-0.094	75	-10.8
CV6	-0.475	-0.103	75	-11.9	-0.448	-0.098	85	-10.6

T1 twin	Orientation of grain:{142.7, 85.9, 12.4}				Orientation of grain:{54.5, 80.8, 7.6}			
	SF	ε_{33}	Length(μm)	$\varepsilon_{33}/\sqrt{L}$	SF	ε_{33}	Length(μm)	$\varepsilon_{33}/\sqrt{L}$
T1V1	-0.022	-0.004	145	-0.3	-0.002	0.000	165	0.0
T1V2	-0.272	-0.048	145	-4.0	-0.303	-0.053	130	-4.7
T1V3	-0.019	-0.003	165	-0.3	-0.006	0.001	155	0.1
T1V4	-0.442	-0.077	140	-6.5	-0.390	-0.068	115	-6.36
T1V5	-0.263	-0.046	145	-3.8	-0.281	-0.049	140	-4.2
T1V6	-0.454	-0.079	130	-7.0	-0.415	-0.073	130	-6.37

Figure 6 shows precisely this effect of domains, in a simpler manner. Each domain will finally have its own dimensions so that new variants could be activated through this size effect (table 7).

In the case of an elongated grain shape, one variant can repeatedly appear several times, as shown in Fig. 7. Although the appearance of the twin changes the dimension of the grain, the size of the free path of this twin remains unchanged, i. e. the favorable orientation (high absolute value of the factor $\frac{\varepsilon_{33}}{\sqrt{L}}$) of this variant remains, therefore it appears repeatedly. With

the increase of the deformation, each twin lamella thickness and finally the whole grain is twinned out.

Table 6: Results for secondary twin

Primary twin is Tension twin T1, secondary twin is compression twin C

T1C	Orientation of grain:{64.4, 161.1, 11.7}				Orientation of grain:{162.4, 20.9, 38.9}			
twin	SF	ε_{33}	Length(μm)	$\varepsilon_{33}/\sqrt{L}$	SF	ε_{33}	Length(μm)	$\varepsilon_{33}/\sqrt{L}$
CV1	-0.295	-0.064	125	-5.7	-0.478	-0.104	180	-7.77
CV2	-0.357	-0.078	128	-6.9	-0.370	-0.081	135	-6.94
CV3	-0.471	-0.103	110	-9.8	-0.209	-0.046	155	-3.67
CV4	-0.488	-0.106	160	-8.4	-0.247	-0.054	105	-5.25
CV5	-0.441	-0.096	110	-9.2	-0.414	-0.09	105	-8.82
CV6	-0.229	-0.05	180	-3.7	-0.471	-0.103	115	-9.57

Primary twin is Compression Twin C, secondary twin is Tension twin T1

CT1	Orientation of grain:{144.6, 82.2, 12.8}				Orientation of grain:{32.4, 77, 39.1}			
twin	SF	ε_{33}	Length(μm)	$\varepsilon_{33}/\sqrt{L}$	SF	ε_{33}	Length(μm)	$\varepsilon_{33}/\sqrt{L}$
T1V1	-0.017	-0.003	50	-0.4	-0.175	-0.031	15	-7.9
T1V2	-0.263	-0.046	20	-10.3	-0.042	-0.007	15	-1.9
T1V3	-0.012	-0.002	20	-0.5	-0.151	-0.026	25	-5.3
T1V4	-0.426	-0.075	25	-14.9	-0.417	-0.073	35	-12.3
T1V5	-0.246	-0.043	35	-7.3	-0.028	-0.005	10	-1.6
T1V6	-0.448	-0.078	30	-14.3	-0.455	-0.08	50	-11.3

Table 7:Domain effect on selection variant (fig 6)

	Orientation of grain:{65.3, 173, 49.2} (Grain initial)				Orientation of grain:{65.3, 173, 49.2} (Domain 2)			
	SF	ε_{33}	Length(µm)	$\varepsilon_{33}/\sqrt{L}$	SF	ε_{33}	Length(µm)	$\varepsilon_{33}/\sqrt{L}$
CV1	-0.386	-0.084	110	-8.03	-0.386	-0.084	55	-11.36
CV2	-0.461	-0.1	70	-12.00	-0.461	-0.1	70	-12.00
CV3	-0.489	-0.107	110	-10.17	-0.489	-0.107	55	-14.38
CV4	-0.475	-0.104	80	-11.59	-0.475	-0.104	50	-14.66
CV5	-0.426	-0.093	70	-11.11	-0.426	-0.093	70	-11.11
CV6	-0.407	-0.089	85	-9.63	-0.407	-0.089	50	-12.56

Once growth achieved, only new twins will appear (compression if tension has been the primary twin and vice versa). For a given orientation, the selection of variants always follows the $\frac{\varepsilon_{33}}{\sqrt{L}}$ criterion. Different types of variant selection can occur in the new grain (fig 7c) but it can always be explained by introducing the concept of domain.

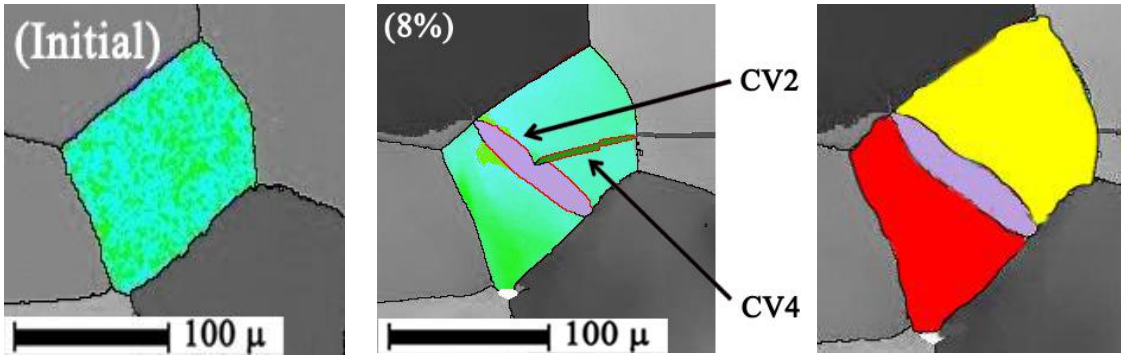

a) Orientation of the matrix:(65.3, 173, 49.2)

b) Compressive twins:CV2 and CV4

c) Domains after the first twin CV2
In red domain 1, in yellow domain 2 and the twin which is the domain 3.

Figure 6: Domain effect on selection variant.

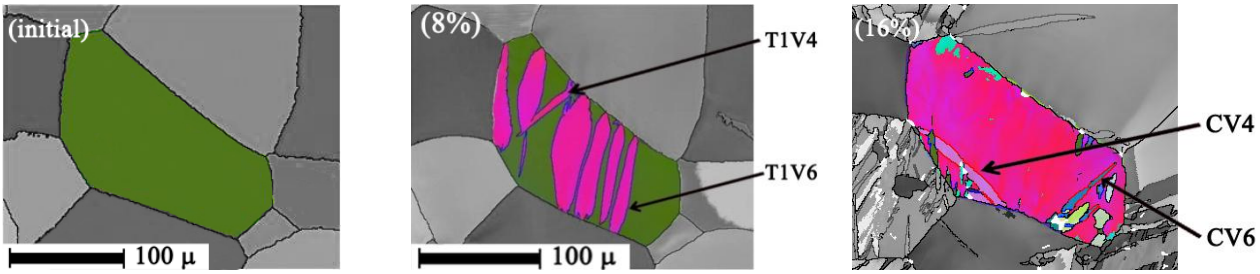

a) Orientation Matrix :(54.5, 80.8, 7.6)

b)Tension twin : T1V4 and T1V6

c) Orientation Matrix :(162.4, 20.9, 38.9)
Compression twin : CV6 and CV1

Figure 7: Long grain a) initial ; b) after 8 % of deformation and c) after 16%

Discussion

The above results demonstrate that the selection of twin variants is strongly dependent on the energy consumed to activate the twin, the mean free path that the twin covers and the shape of the initial grain. Once a twin forms in a grain, it cuts the grain and thus inevitably changes the dimensions of this grain, subdividing the initial grain into three domains. The twin can be regarded as a new grain with its own dimension and crystallographic orientation. Each time when a twin forms, the size of the parent grain is modified and thus the apparent stress on each possible twin variant will change according to the HP law. As a result, variants which did not have a sufficient level of stress through the SF can nevertheless be active in a newly created domain, despite the orientation of the initial grain not having changed. This explains why in equiaxed grains, several variants can appear. However, in the elongated grains, although the activation of the twin variant changes the dimension of the grain, it does not change the length of the free path of this variant. Thus this variant can form repeatedly as long as it does not create conditions more favorable for another variant. In such conditions, the twins activated can continue to grow until the whole grain is twinned out.

A twin can thus be regarded as a new grain, which is a slightly different point of view than that of secondary twin. Generally, this new grain presents an elongated shape (at least at the early stage of its formation). Thus there will generally be, one activated variant in this existing twin. In fact, this notion strongly depends on the size of the twin, since, it was seen that when a grain is fully consumed by twinning there can be several variants thereafter.

When several twin variants, that do not cross the grain right through, form in one grain, the grain is divided into domains. A domain is thus limited by twin boundaries and grain boundaries. Each domain has its own crystallographic orientation (generally that of the matrix) and its own dimensions.

Currently, it is not possible to have an absolute prediction because interactions between neighbors (local field stresses and deformations) is not taken into account. This effect (of neighbors) is visible in Figure 3b, where the variant CV1 came at the top left of the grain. In addition, we have a surface vision of a volume phenomenon. Similarly the comparison with experimental measurement is only on a surface (2D) but the twins growth in the volume of the grain (in 3D)

Conclusion

With the experimental examination, an energetic twin variant selection rule in titanium during deformation has been proposed. The prediction is correct in 85% of the cases, whereas that according to Schmid factor only in 50%.

For the time being, this rule has been verified with the (1012) and (1122) twins that are frequent in titanium and titanium alloys. For (1121) twin, if the constants used in the Hall-Petch relation are determined, this rule can also be applied. The rule can be used to calculate the energy consumption for twin formation, i.e. the internal energy consumed to form a

twin. The choice of a slip or twinning system is only based on an energy criterion. The system used will be that which will make it possible to lower as much as possible the internal energy of the material.

Calculations by ab-initio and EAM methods are undertaken to determine twinning energies. These calculations already led to results in the case of crystallographic slip [25].

Taking account of the grain size seems to be one of the essential keys to explain the variant selection. More precisely, it will introduce the concepts of domain, free path and that of new grain. Thus, a twin will be regarded as a – new - grain characterized by its size and crystallographic orientation. Accordingly, the concept of secondary twinning could be reconsidered.

**Acknowledgement:

This work was supported by the Federation of Research for Aeronautic and Space (Fédération de Recherche pour l'Aéronautique et l'Espace Thème Matériaux pour l'Aéronautique et l'Espace : project OPTIMIST (optimisation de la mise en forme d'alliage de titane)).

Appendix

Expression of displacement tensor in crystal frame

$$\mathbf{X} = \begin{pmatrix} n_1 & p_1 & m_1 \\ n_2 & p_2 & m_2 \\ n_3 & p_3 & m_3 \end{pmatrix} \tag{1}$$

where the basis vector SPN (Shear Plane Normal) can be obtained by the vector cross product of SD (Shear Direction) and HPN (Habit Plane Normal) [26].

$$\mathrm{p} = \mathrm{n} \times \mathrm{m} = \begin{pmatrix} n_1 \\ n_2 \\ n_3 \end{pmatrix} \times \begin{pmatrix} m_1 \\ m_2 \\ m_3 \end{pmatrix} = \begin{pmatrix} m_3 n_2 - m_2 n_3 \\ m_1 n_3 - m_3 n_1 \\ m_2 n_1 - m_1 n_2 \end{pmatrix} \tag{2}$$

By definition, twinned crystals can be obtained by a 180° rotation around either K_1 plane normal (Type I) or η_1 (Type II) of the matrix, shown in Fig. 5. Thus the coordinate transformation between the two crystal bases can be described with following rotation matrix.

$$\mathbf{R}^{\boldsymbol{\theta}}_{[\mathbf{r_1 r_2 r_3}]} = \begin{pmatrix} r_1^2(1-cos\theta)+cos\theta & r_1 r_2(1-cos\theta)-r_3 sin\theta & r_1 r_3(1-cos\theta)+r_2 sin\theta \\ r_2 r_1(1-cos\theta)+r_3 sin\theta & r_2^2(1-cos\theta)+cos\theta & r_2 r_3(1-cos\theta)-r_1 sin\theta \\ r_3 r_1(1-cos\theta)-r_2 sin\theta & r_3 r_2(1-cos\theta)+r_1 sin\theta & r_3^2(1-cos\theta)+cos\theta \end{pmatrix} \tag{3}$$

Where θ is the rotation angle and **r** (r_1, r_2, r_3) the rotation axis. In our case, θ=180°; the rotation axis is the unit vector normal to K_1, as below:

$$\mathbf{R}^{\theta=\pi}_{\mathbf{n}} = \begin{pmatrix} 2n_1^2-1 & 2n_1 n_2 & 2n_1 n_3 \\ 2n_1 n_2 & 2n_2^2-1 & 2n_2 n_3 \\ 2n_1 n_3 & 2n_2 n_3 & 2n_3^2-1 \end{pmatrix} \tag{4}$$

With following matrix multiplication we obtain the tensor displacement (e_{ij}^t) in the crystal basis.

$$\mathrm{E}=\mathrm{X}\left(e_{ij}^t\right)\mathrm{X}^{-1} \tag{5}$$

Or for secondary twin $E=RX(e_{ij}^{t})X^{-1}R^{-1}$ (6)

where

$$(e_{ij}^{t}) = \begin{pmatrix} 0 & 0 & s \\ 0 & 0 & 0 \\ 0 & 0 & 0 \end{pmatrix} \quad (7)$$

which is the tensor displacement in the twin reference frame.

Eq. (5) expresses the tensor displacement of the primary twin in the crystal basis of the parent matrix and Eq. (6) expresses the tensor displacement of the secondary twin in the crystal basis of the parent matrix.

References:

[1] Kocks, U.F. and D.G. Westlake, *The importance of twinning for the ductility of HCP polycrystals.* AIME MET SOC TRANS, 1967. **239**(7): p. 1107-1109.

[2] Yoo, M., *Slip, twinning, and fracture in hexagonal close-packed metals.* Metallurgical and Materials Transactions A, 1981. **12**(3): p. 409-418.

[3] Philippe, M.J., et al., *Modelling of texture evolution for materials of hexagonal symmetry--II. application to zirconium and titanium [alpha] or near [alpha] alloys.* Acta Metallurgica et Materialia, 1995. **43**(4): p. 1619-1630.

[4] Chun, Y.B., et al., *Effect of deformation twinning on microstructure and texture evolution during cold rolling of CP-titanium.* Materials Science and Engineering A, 2005. **398**(1-2): p. 209-219.

[5] Shin, D.H., et al., *Shear strain accommodation during severe plastic deformation of titanium using equal channel angular pressing.* Materials Science and Engineering A, 2002. **334**(1-2): p. 239-245.

[6] Bao, L., et al., *Study of Plastic Deformation in Hexagonal Metals by Interrupted In-Situ EBSD Measurement.* Advanced Engineering Materials, 2010. **12**(10): p. 1053-1059.

[7] Crocker, A.G., *The crystallography of deformation twinning in alpha-uranium.* Journal of Nuclear Materials, 1965. **16**(3): p. 306-326.

[8] Mahajan, S. and D.F. Williams, *Deformation twinning in metals and alloys.* International Metallurgical Reviews, 1973. **18**: p. 43-61.

[9] Akhtar, A., *Basal slip and twinning in a-titanium single crystals.* Metallurgical and Materials Transactions A, 1975. **6**(4): p. 1105-1113.

[10] Ishiyama, S., S. Hanada, and O. Izumi, *Orientation Dependence of Twinning in Commercially Pure Titanium.* Journal of the Japan Institute of Metals, 1990. **54**(9): p. 976-984.

[11] Churchman, A.T., *The formation and removal of twins in titanium during deformation.* J. Inst. Metals, 1954. **83**: p. 39-40.

[12] Song, S.G. and G.T. Gray, *Structural interpretation of the nucleation and growth of deformation twins in Zr and Ti--II. Tem study of twin morphology and defect reactions during twinning.* Acta Metallurgica et Materialia, 1995. **43**(6): p. 2339-2350.

[13] Goo, E. and K.T. Park, *Application of the von Mises Criterion to Deformation Twinning.* Scripta metallurgica, 1989. **23**(7): p. 1053-1056.

[14] Proust, G., C.N. Tomé, and G.C. Kaschner, *Modeling texture, twinning and hardening evolution during deformation of hexagonal materials.* Acta Materialia, 2007. **55**(6): p. 2137-2148.

[15] Wu, X., et al., *Prediction of crystallographic texture evolution and anisotropic stress-strain curves during large plastic strains in high purity [alpha]-titanium using a Taylor-type crystal plasticity model.* Acta Materialia, 2007. **55**(2): p. 423-432.

[16] Wonsiewicz, B.C. and W.A. Backofen, *Independent slip systems and ductility of hexagonal polycrystals.* Transactions of The Metallurgical Society of AIME, 1967. **239**.

[17] Partridge, P.G., *The crystallography and deformation modes of hexagonal close-packed metals.* Metallurgical Reviews, 1967. **12**(118): p. 169-194.

[18] Meyers, M.A., O. Vöhringer, and V.A. Lubarda, *The onset of twinning in metals: a constitutive description.* Acta Materialia, 2001. **49**(19): p. 4025-4039.

[19] Philippe, M.J., C. Esling, and B. Hocheid, *Role of Twinning in Texture Development and in Plastic Deformation of Hexagonal Materials.* Textures and Microstructures, 1988. **7**: p. 265-301.

[20] Fundenberger, J.J., et al., *Modelling and prediction of mechanical properties for materials with hexagonal symmetry (zinc, titanium and zirconium alloys).* Acta Materialia, 1997. **45**(10): p. 4041-4055.

[21] Mason, T., et al., *Advances in deformation twin characterization using electron backscattered diffraction data.* Metallurgical and Materials Transactions A, 2002. **33**(13): p. 949-954.

[22] Bao, L., et al., *Study of Deformation Mechanisms in Titanium by Interrupted Rolling and Channel Die Compression Tests.* Computers, Materials, & Continua, 2010. **15**(2): p. 113-128.

[23] Lebensohn, R.A. and G.R. Canova, *A self-consistent approach for modelling texture development of two-phase polycrystals application to titanium alloys.* Journal Name: Acta Materialia; Journal Volume: 45; Journal Issue: 9; Other Information: PBD: Sep 1997, 1997: p. 3687-3694.

[24] Le Cras, F. et al., *Determination of experimental and Modelized flow field for a titanium alloy during cold rolling.* Proceeding Titanium 95, vol. 1, p 659

[25] Poty, A. et al., *Classification of the Critical Resolved Shear Stress in the HCP materials by atomic simulation: Application to zirconium and titanium*. Journal of Applied Physics (accepted, to be publish)

[26] Martin, E et al., *Variant selection during secondary twinning in Mg–3%Al,* Acta Materialia, Volume 58, Issue 11 June 2010, p 3970

[27] Jonas, J.J. et al., *The role of strain accommodation during the variant selection of primary twins in magnesium,* Acta Materialia, Volume 59, Issue 5, March 2011, p 2046